Chapter 26

3D and 4D Heteronuclear Magnetic Resonance

G. Marius Clore and Angela M. Gronenborn

Laboratory of Chemical Physics, Bldg 5/B1-30I, Protein NMR Section, NIDDK, National Institutes of Health, Bethesda, MD 20892-0520, USA

26.1 WHY ARE THREE- (3D) AND FOUR-DIMENSIONAL (4D) EXPERIMENTS REQUIRED?

The principal source of geometric information used to solve 3D structures of macromolecules by NMR resides in short (<5 Å), approximate, interproton distance restraints derived from nuclear Overhauser enhancement (NOE) measurements.[1–7] To extract this information, first, it is essential to completely assign the ^{1}H spectrum of the macromolecule in question and then to assign as many structurally useful NOE interactions as possible. The larger the number of NOE restraints, the higher the precision and the accuracy of the resulting structures.[7–9] Indeed, with current state-of-the-art methodology, it is now possible to obtain NMR structures of proteins at a precision and accuracy approximately comparable to that of 2 Å resolution crystal structures.[8–12] For proteins of 100 residues or less, conventional homonuclear 2D NMR methods can be applied with a considerable degree of success.[1–7,13,14] As the number of residues and molecular weight increase beyond 100 and 12 kDa, respectively, there are two main obstacles, which have made it necessary to extend the 2D NMR techniques to higher dimensions and to develop new approaches. First, the increased spectral complexity arising from the presence of a larger number of protons results in extensive chemical shift overlap and degeneracy, rendering the 2D spectra uninterpretable. Second, the rotational correlation time increases with increase in molecular weight, resulting in large ^{1}H linewidths and a concomitant severe decrease in the sensitivity of correlation experiments based on intrinsically small three-bond ^{1}H–^{1}H couplings. These obstacles can be overcome by increasing the dimensionality of the spectra to resolve problems associated with spectral overlap and by simultaneously making use of heteronuclear couplings that are larger than the linewidths to

circumvent limitations in sensitivity.[8,9] This approach necessitates uniform ^{15}N and/or ^{13}C labeling of the macromolecule under consideration.

The concept of increasing spectral dimensionality to extract information can perhaps most easily be understood by analogy.[8] Consider, for example, the Encyclopedia of Magnetic Resonance. In a 1D representation, all the information (i.e., words and sentences arranged in a particular set order) present in the Encyclopedia of Magnetic Resonance would be condensed into a single line. If this line were expanded to two dimensions in the form of a page, the odd word might be resolved but the vast majority would still be superimposed on each other. When this page is expanded into a book (i.e., three dimensions) comprising a set number of lines and words per page, as well as a fixed number of pages, some pages may become intelligible, but many words will still lie on top of each other. The final expansion to the multivolume book (i.e., four dimensions) then makes it possible to extract in full all the information present in the individual entries of the Encyclopedia of Magnetic Resonance.

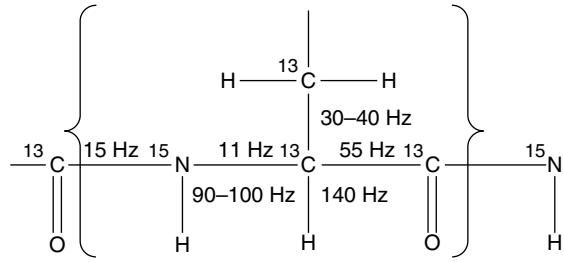

Figure 26.2. Summary of the one-bond heteronuclear couplings along the polypeptide chain utilized in 3D and 4D NMR experiments.

26.2 The Design and Implementation of 3D and 4D Experiments

The design and implementation of higher dimensionality NMR experiments can be carried out by the appropriate combination of 2D NMR experiments, as illustrated schematically in Figure 26.1. A 3D experiment is constructed from two 2D pulse schemes by leaving out the detection period of the first experiment and the preparation pulse of the second one.[15] This results in a pulse train comprising two independently incremented evolution periods t_1 and t_2, two corresponding mixing periods M_1 and M_2, and a detection period t_3. Similarly, a 4D experiment is obtained by combining three 2D experiments in an analogous manner. Thus, conceptually n-dimensional NMR can be conceived as a straightforward extension of 2D NMR. The real challenge, however, of 3D and 4D NMR is twofold: first, to ascertain which 2D experiments should be combined to best advantage and second, to design the pulse sequences in such a way that undesired artifacts, which may severely interfere with the interpretation of the spectra, are removed. This task is far from trivial.

Heteronuclear 3D and 4D NMR experiments exploit a series of large one-bond heteronuclear couplings for magnetization transfer through bonds that are summarized in Figure 26.2. This, together with the fact that the ^1H nucleus is always detected, renders these experiments very sensitive. Indeed, high-quality 3D and 4D heteronuclear-edited spectra can easily be obtained on samples of 1–2 mM uniformly labeled protein in a timeframe that is limited solely by the number of increments that have to be collected for appropriate digitization and the number of phase cycling steps that have to be used to reduce artifacts to an acceptably low level. A detailed technical review of heteronuclear multidimensional NMR has been provided by Clore and Gronenborn.[16]

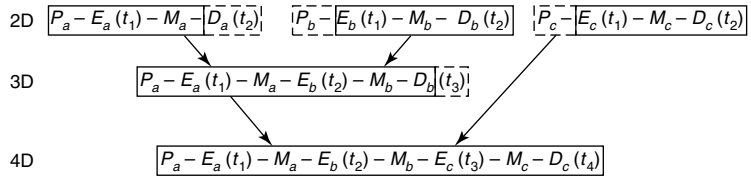

Figure 26.1. General representation of pulse sequences used in multidimensional NMR illustrating the relationship between the basic schemes used to record 2D, 3D, and 4D NMR spectra. Note how 3D and 4D experiments are constructed by the appropriate linear combination of 2D ones. Abbreviations: P, preparation; E, evolution; M, mixing; and D, detection. In 3D and 4D NMR, the evolution periods are incremented independently.

26.3 Heteronuclear Editing of $^1H-^1H$ Experiments

Many of the 3D and 4D experiments are based on heteronuclear editing of $^1H-^1H$ experiments so that the general appearance of conventional 2D experiments is preserved and the total number of cross peaks present is the same as that in the 2D equivalents.[8,9,16–24] The progression from a 2D spectrum to 3D and 4D heteronuclear-edited spectra is depicted schematically in Figure 26.3. Consider, for example, the cross peaks involving a particular ^1H frequency in a 2D NOESY spectrum, a 3D ^{15}N or ^{13}C-edited NOESY spectrum, and finally a 4D $^{15}N/^{13}C$ or $^{13}C/^{13}C$-edited NOESY spectrum. In the 2D spectrum, a series of cross peaks will be seen from the originating proton frequencies in the F_1 dimension to the single destination ^1H frequency along the F_2 dimension. From the 2D experiment, it is impossible to ascertain whether these NOEs involve only a single destination proton or several destination protons with identical chemical shifts. By spreading the spectrum into a third dimension according to the chemical shift of the heteronucleus attached to the destination proton(s), NOEs involving different destination protons will appear in distinct $^1H-^1H$ planes of the 3D spectrum. Thus, each interaction is simultaneously labeled by three chemical shift coordinates along three orthogonal axes of the spectrum. The projection of all these planes onto a single plane yields the corresponding 2D spectrum. For the purposes of sequential assignment, heteronuclear-edited 3D spectra are often sufficient for analysis. However, when the goal of the analysis is to assign NOEs between protons far apart in the sequence, a 3D ^{15}N- or ^{13}C-edited NOESY spectrum will often prove inadequate. This is because the originating protons are only specified by their ^1H chemical shifts, and more often than not, there are several protons that resonate at the same frequencies. For example, in the case of the 153-residue protein interleukin-1β, there are about 60 protons that resonate in a 0.4 ppm interval between 0.8 and 1.2 ppm. Such ambiguities can then be resolved by spreading out the 3D spectrum still further into a fourth dimension according to the chemical shift of the heteronucleus attached to the originating protons, so that each NOE interaction is simultaneously labeled by four chemical shift coordinates along four orthogonal axes, namely, those of the originating and destination protons and those of the corresponding heteronuclei directly bonded to these protons.[25–27] The result is a

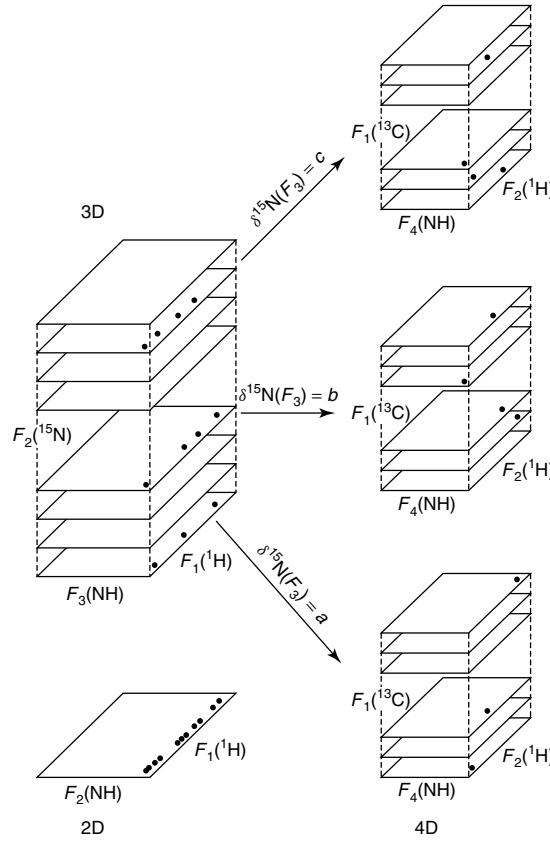

Figure 26.3. Schematic illustration of the progression and relationship between 2D, 3D, and 4D heteronuclear NMR experiments. The solid circles represent NOE cross peaks. In the example shown, there are 11 NOEs originating from 11 different protons in the F_1 dimension to a single-frequency position in the F_2 dimension. In the 2D spectrum, it is impossible to ascertain whether there is only one destination proton or several in the F_2 dimension. By spreading the spectrum into a third dimension (labeled F_3), according to the chemical shift of the heteronucleus attached to the destination proton, it can be seen that the NOEs now lie in three distinct $^1H(F_1)-^1H(F_3)$ planes, indicating that three different destination protons are involved. However, the ^1H chemical shifts still provide the only means of identifying the originating protons. Hence, the problem of spectral overlap still prevents the unambiguous assignment of these NOEs. By extending the spectrum to 4D, each NOE interaction is labeled by four chemical shifts along four orthogonal axes. Thus, the NOEs in each plane of the 3D spectrum are now spread over a cube in the 4D spectrum according to the chemical shift of the heteronucleus directly attached to the originating protons. (Reproduced from Ref. 25. © American Association for the Advancement of Science (AAAS).)

4D spectrum in which each plane of the 3D spectrum constitutes a cube in the 4D spectrum.

26.4 COMPARISON OF 2D, 3D, AND 4D EXPERIMENTS

For illustration purposes, it is also useful to compare the type of information that can be extracted from a very simple system using 2D, 3D, and 4D NMR. Consider a molecule with only two NH and two aliphatic protons in which only one NH proton is close to an aliphatic proton. In addition, the chemical shifts of the NH protons are degenerate, as are those of the aliphatic protons, so that only two resonances are seen in the 1D spectrum. In the 2D NOE spectrum, an NOE will be observed between the resonance position of the NH protons and the resonance position of the aliphatic protons, but it will be impossible to ascertain which one of the four possible NH–aliphatic-proton combinations gives rise to the NOE. By spreading the spectrum into a third dimension, for example, by the chemical shift of the ^{15}N atoms attached to the NH protons, the number of possibilities will be reduced to two, provided that the chemical shifts of the two nitrogen atoms are different. Finally, when the fourth dimension corresponding to the chemical shift of the ^{13}C atoms attached to the aliphatic protons is introduced, a unique assignment of the NH–aliphatic-proton pair giving rise to the NOE can be made.

Figure 26.4(a) presents a portion of the 2D ^{15}N-edited NOESY spectrum of interleukin-1β (153 residues), illustrating NOE interactions between the NH protons along the F_2 axis and the CαH protons along the F_1 dimension.[19] Despite the fact that a large number of cross peaks can be resolved, it can be seen that many of the cross peaks have identical chemical shifts in one or other dimensions. For example, there are 15 cross peaks involving NH protons at an $F_2(^1\text{H})$ chemical shift of <9.2 ppm. A single $^1\text{H}(F_1)$–$^1\text{H}(F_3)$ plane of the 3D ^{15}N-edited NOE spectrum of interleukin-1β at $\delta^{15}\text{N}(F_2) = 123.7$ ppm is shown in Figure 26.4(b). Not only is the number of cross peaks in this slice small, but also at $\delta^1\text{H}(F_3)$ <9.2 ppm there is only a single cross peak involving one NH proton. The correlations observed in the ^{15}N-edited NOE spectrum are through-space ones. Intraresidue correlations from the NH protons to the CαH and CβH protons can similarly be resolved using a 3D ^{15}N-edited HOHAHA spectrum in which efficient isotropic mixing sequences are used to transfer magnetization between protons via three-bond ^1H–^1H couplings.

The 3D ^{15}N-edited NOESY and HOHAHA spectra constitute only one of several versions of a 3D heteronuclear-edited spectrum. Many alternative through-bond pathways can be utilized to great effect. Consider, for example, the delineation amino acid spin systems that involve grouping those resonances that belong to the same residue. In 2D NMR, correlation experiments are used to delineate either direct or relayed connectivities via small three-bond ^1H–^1H couplings. Even for proteins of 50–60 residues, it can be difficult to delineate long-chain amino acids such as lysine (Lys) and arginine (Arg) in this manner. In heteronuclear 3D NMR, an alternative pathway can be employed, which involves transferring magnetization first from a proton to its directly attached carbon atom systems via the large ^1J(C,H) coupling (<130 Hz), followed by either direct or relayed transfer of magnetization along the carbon chain via the ^1J(C,C) couplings (<30–40 Hz), before transferring the magnetization back to protons.[31–33] An example of such a spectrum is the so-called HCCH-TOCSY shown in Figure 26.4(c). The $^1\text{H}(F_1)$–$^1\text{H}(F_3)$ plane at $\delta^{13}\text{C}$ $(F_2) = 59$ ppm illustrates both direct and relayed connectivities along various side chains originating from CαH protons. As expected, the resolution of the spectrum is excellent and there is no spectral overlap. Just as importantly, however, the sensitivity of the experiment is extremely high and complete spin systems are readily identified in interleukin-1β even for long side chains, such as those of two Lys residues shown in the figure. Indeed, by analyzing spectra of this kind, it was possible to obtain complete ^{1}H and ^{13}C assignments for the side chains.[16,34,35]

3D NMR also permits one to devise a whole range of correlation experiments on the basis of through-bond heteronuclear connectivities for sequential assignment. The connectivities observed in these correlation experiments are entirely predictable. In contrast, the NOE relies solely on close proximity of protons, and it may, therefore, be possible to confuse sequential connectivities with long-range ones. These 3D heteronuclear correlation experiments are of the triple-resonance variety and make use of one-bond $^{13}\text{CO}(i-1)$–$^{15}\text{N}(i)$, $^{15}\text{N}(i)$–$^{13}\text{C}\alpha(i)$,

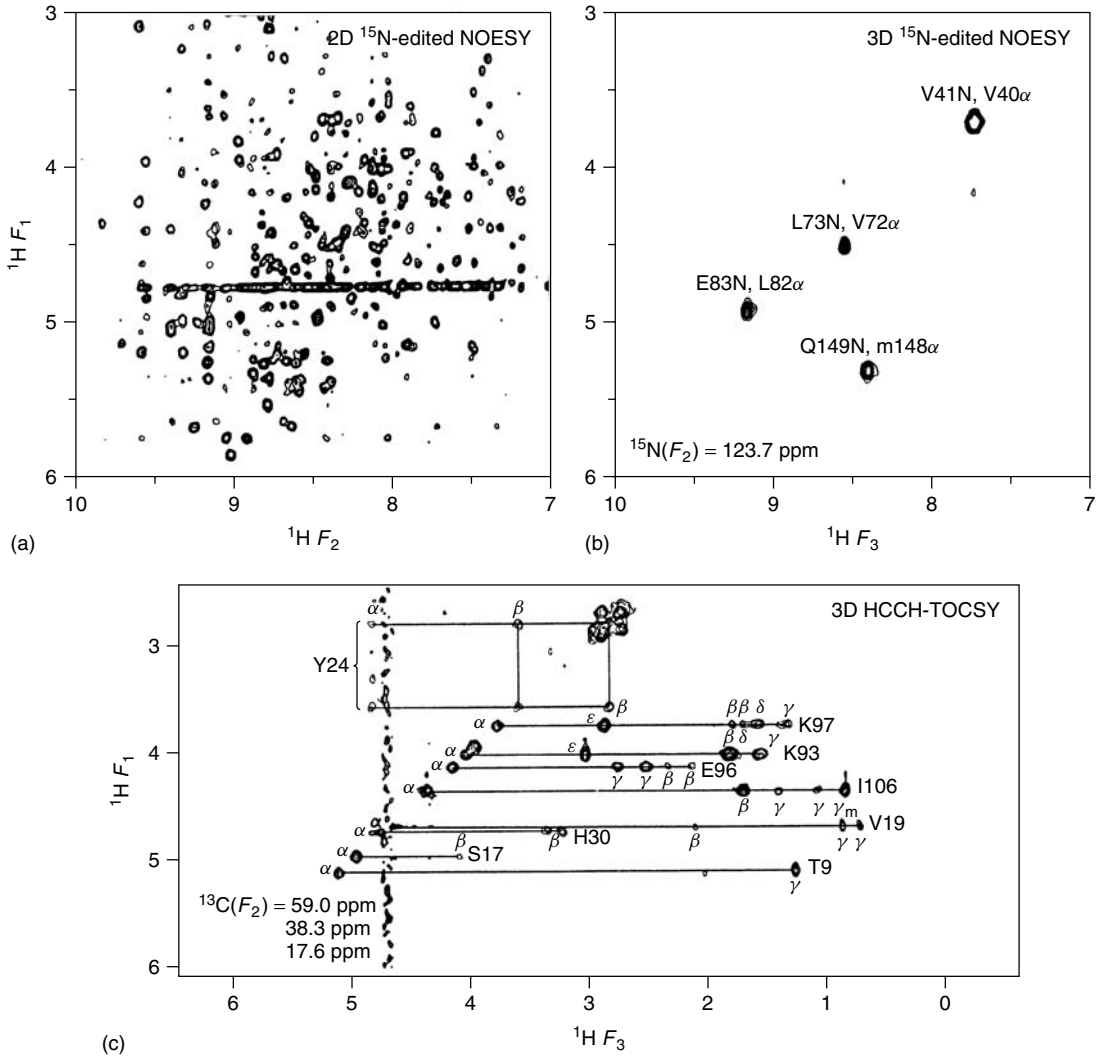

Figure 26.4. Example of 2D and 3D spectra of interleukin-1β recorded at 600 MHz.[19,28–30] The 2D spectrum in (a) shows the NH(F_2 axis)–CαH(F_1 axis) region of a 2D ^{15}N-edited NOE spectrum. The same region of a single NH(F_3)–^{1}H(F_1) plane of the 3D ^{15}N-edited NOE at δ^{15}N(F_2) = 123.7 ppm is shown in (b). The actual 3D spectrum comprises 64 such planes and projection of these on a single plane would yield the same spectrum as in (a). Part (c) shows a single ^{1}H(F_3)–^{1}H(F_1) plane of the 3D HCCH-TOCSY spectrum at δ^{13}C(F_2) = 38.3 ± nSW (where SW is the spectral width of 20.71 ppm in the ^{13}C dimension) illustrating both direct and relayed connectivities originating from the Cα,H protons. Note how easy it is to delineate complete spin systems of long side chains such as Lys (i.e. cross peaks to the Cβ,H, CγH, CδH, and CαH protons are observed) owing to the fact that magnetization along the side chain is transferred via large ^1J(C,C) couplings. Several features of the HCCH-TOCSY spectrum should be pointed out. First, extensive folding is employed which does not obscure analysis as ^{13}C chemical shifts for different carbon types are located in characteristic regions of the ^{13}C spectrum with little overlap. Second, the spectrum is edited according to the chemical shift of the heteronucleus attached to the originating proton rather than the destination one. Third, multiple cross checks on the assignments are readily made by looking for the symmetry-related peaks in the planes corresponding to the ^{13}C chemical shifts of the destination protons in the original slice.

Table 26.1. Summary of correlations observed in the 3D double and triple resonance experiments used for sequential and side-chain assignments

Experiment	Correlation	J-coupling
^{15}N-edited HOHAHA	C-α,H(i)–^{15}N(i)–NH(i)	^{3}J(H,N-α) (≈3–11 Hz)
	C-β,H(i)–^{15}N(i)–NH(i)	^{3}J(H,N-α) (≈3–11 Hz) and $^{3}J(\alpha, \beta)$ (≈3–11 Hz)
H(CA)NH	C-α,H(i)–^{15}N(i)–NH(i)	^{1}J(N,C-α) (≈9–13 Hz)
	C-α,H($i-1$)–^{15}N(i)–NH(i)	^{2}J(N,C-α) (≈5–10 Hz)
HN(CO)HB	C-α,H($i-1$)–^{15}N(i)–NH(i)	^{2}J(CO,H-α) (≈4–7 Hz)
	C-β,H($i-1$)–^{15}N(i)–NH(i)	^{3}J(CO,H-β) (≈8 Hz for *trans* coupling)
HNHB	C-β,H(i)–^{15}N(i)–NH(i)	^{3}J(N,H-β) (≈5 Hz for *trans* coupling)
HNCA	^{13}C-α(i)–^{15}N(i)–NH(i)	^{1}J(N,C-α) (≈9–13 Hz)
	^{13}C-α($i-1$)–^{15}N(i)–NH(i)	^{2}J(N,C-α) (≈5–10 Hz)
CBCANH	^{13}C-β/C-α(i)–^{15}N(i)–NH(i)	^{1}J(C,C) (≈30–40 Hz), ^{1}J(N,C-α) (≈9–13 Hz)
	^{13}C-β/C-α($i-1$)–^{15}N(i)–NH(i)	^{1}J(C,C) (≈30–40 Hz), ^{2}J(N,C-α) (≈5–10 Hz)
HN(CO)CA	^{13}C-α($i-1$)–^{15}N(i)–NH(i)	^{1}J(N,CO) (≈15 Hz) and ^{1}J(C-α,CO) (≈55 Hz)
CBCA(CO)NH	^{13}C-β/C-α($i-1$)–^{15}N(i)–NH(i)	^{1}J(C,C) (≈30–40 Hz), ^{1}J(N,CO) (≈15 Hz), and ^{1}J(C-α,CO) (≈55 Hz)
HBHA(CO)NH	C-β,H/C-α,H($i-1$)–^{15}N(i)–NH(i)	^{1}J(C,C) (≈30–40 Hz), ^{1}J(N,CO) (≈15 Hz), and ^{1}J(C-α,CO) (≈55 Hz)
C(CO)NH	^{13}C-x,($i-1$)–^{15}N(i)–NH(i)	^{1}J(C,C) (≈30–40 Hz), ^{1}J(N,CO) (≈15 Hz), and ^{1}J(C-α,CO) (≈55 Hz)
H(CCO)NH	C-x,H($i-1$)–^{15}N(i)–NH(i)	^{1}J(C, C) (≈30–40 Hz), ^{1}J(N,CO) (≈15 Hz), and ^{1}J(C-α,CO) (≈55 Hz)
HNCO	^{13}CO($i-1$)–^{15}N(i)–NH(i)	^{1}J(N,CO) (≈15 Hz)

^{13}C(i)–^{13}C(i), and ^{13}Cα(i)–^{13}CO(i) couplings, as well as two-bond ^{13}Cα($i-1$)–^{15}N(i) couplings. In this manner multiple, independent pathways for linking the resonances of one residue with those of its adjacent neighbor are available, thereby avoiding ambiguities in the sequential assignment (Table 26.1).

In practice, only a limited number of 3D triple and double resonance experiments need to be performed to obtain complete assignments. In our experience, the following eight 3D experiments not only provide all the information required but are also characterized by high sensitivity and can be recorded in as little as 2 weeks of measuring time. Specifically, the 3D CBCA(CO)NH and HBHA(CBCACO)NH experiments[36,37] are used to correlate the chemical shifts of Cα/Cβ($i-1$) and Hα/Hβ($i-1$), respectively, of residue $i-1$ with the ^{15}N(i)/NH(i) chemical shifts of the residue i; and the complementary 3D C(CO)NH and H(CCO)NH experiments[38] are used to correlate the chemical shifts of the aliphatic side-chain ^{13}C and ^{1}H resonances, respectively, of the residue $i-1$ with the ^{15}N(i)/NH(i) chemical shifts of the residue i. In the first two experiments, magnetization originating on Cβ is transferred to Cα by a COSY mixing pulse, whereas in the second pair of experiments, magnetization is transferred from a side-chain C atom along the carbon chain to Cα via isotropic mixing. Intraresidue correlations to the NH group can be obtained from the 3D CBCANH[39] and ^{15}N-edited HOHAHA[40] experiments. The 3D CBCANH experiment correlates the chemical shifts of Cα(i)/Cβ(i) (as well as those of Cα($i-1$)/Cβ($i-1$), which invariably give rise to weaker cross peaks), with the ^{15}N(i)/NH(i) chemical shifts of the residue i; the 3D ^{15}N-separated HOHAHA experiment correlates the chemical shifts of the side-chain protons of the residue i with the ^{15}N(i)/NH(i) chemical shifts of the residue i. Finally, the 3D HCCH-COSY and HCCH-TOCSY experiments[31,33] can be used to confirm and obtain complete ^{1}H and ^{13}C assignments of the side chains.

The power of 4D heteronuclear NMR spectroscopy for unraveling interactions that would not have been possible in lower dimensional spectra is illustrated in Figure 26.5 by the ^{13}C/^{13}C-edited NOESY spectrum of interleukin-1β.[26] Figure 26.5(a)

shows a small portion of the aliphatic region between 1 and 2 ppm of a conventional 2D NOESY spectrum of interleukin-1β. The overlap is so great that no single, individual cross peak can be resolved. One might, therefore, wonder just how many NOE interactions are actually superimposed, for example, at the ^{1}H chemical shift coordinates of the letter X at 1.39 (F_1) and 1.67 (F_2) ppm.

A ^{1}H(F_2)–^{1}H(F_4) plane of the 4D spectrum at δ^{13}C(F_1), δ^{13}C(F_3) = 44.3 ppm, 34.6 ppm is shown in Figure 26.5(b) and the square box at the top right-hand side of this panel encloses the region between 1 and 2 ppm. Only two cross peaks are present in this region, and the arrow points to a single NOE between the CγH and CβH protons of Lys-77 with the same ^{1}H chemical shift coordinates as the letter X in panel A. All the other NOE interactions at the same ^{1}H chemical shift coordinates can be determined by inspection of a single ^{13}C(F_1)–^{13}C(F_3) plane taken at δ^1H(F_2), δ^1H(F_4) = 1.39 ppm, 1.67 ppm. This reveals a total of seven NOE interactions superimposed at the ^{1}H chemical shift coordinates of the letter X. Another feature of the 4D spectrum is illustrated by the two ^{1}H(F_2)–^{1}H(F_4) planes at different F_1 and F_3 ^{13}C frequencies shown in Figure 26.5(c) and (b). In both cases, there are cross peaks involving protons with identical or near-identical chemical shifts, namely, that between praline (Pro)-91(CαH) and tyrosine (Tyr)-90(CαH), diagnostic of a *cis*-Pro, shown in Figure 26.5(c), and between phenylalanine (Phe)-99(CβH) and methionine (Met)-95(CγH) shown in Figure 26.5(d). These interactions could not be resolved in either a 2D spectrum or a 3D ^{13}C-edited spectrum as they would lie on the spectral diagonal (i.e., the region of the spectrum corresponding to magnetization that has not been transferred from one proton to another). In the 4D spectrum, however, they are easy to observe, provided that the ^{13}C chemical shifts of the directly bonded ^{13}C nuclei are different. Because the number of NOE interactions present in each ^{1}H(F_4)–^{1}H(F_2) plane of 4D ^{13}C/^{15}N or ^{13}C/^{13}C-edited NOE spectra is so small, the inherent resolution in a 4D spectrum is extremely high, despite the low level of digitization. Indeed, spectra with equivalent resolution can be recorded at magnetic field strengths considerably lower than 600 MHz, although this would obviously lead to a reduction in sensitivity. Further, it can be calculated that 4D spectra with virtual lack of resonance overlap and good sensitivity can be obtained on proteins with as many as 400 residues. Thus, once complete ^{1}H, ^{15}N, and ^{13}C assignments are obtained, analysis of 4D spectra should permit the automated assignment of almost all NOE interactions.

26.5 BRIEF OVERVIEW OF DEVELOPMENTS SINCE 1996

During the last decade, on large systems, NMR has benefited enormously from the application of transverse relaxation-optimized spectroscopy (TROSY)-based experiments.[43] NMR studies of very large molecules, complexes, and assemblies become increasingly more difficult due to increased linewidths associated with slower tumbling, as well as even more pronounced spectral overlap. In conventional heteronuclear correlation spectra (e.g., HSQC), large heteronuclear couplings between spins, such as ^{15}N–^{1}H^N or ^{13}C–^{1}H, are exploited for magnetization transfer. These scalar couplings give rise to multiplet components with different relaxation properties. In decoupled HSQC spectra, only a single signal is obtained for each spin pair; as a consequence, relaxation properties are averaged among the multiplet components. The TROSY advantage is based on the fact that for large systems (i.e., slower tumbling molecules), narrower lines and higher sensitivity can be obtained by selecting the slowly relaxing components of ^{15}N–^{1}H^N or ^{13}C–^{1}H antiphase coherences, omitting the other faster relaxing components. The resulting narrower linewidths have led to widespread use of TROSY, and the TROSY principle has been incorporated into all the commonly used pulse schemes. In particular, TROSY double and triple-resonance experiments exhibit superior sensitivity and spectral resolution relative to their conventional counterparts, particularly if the protein of interest is deuterated.[44] The basic principles and applications of 3D and 4D TROSY-based triple-resonance and NOE experiments for structure-function studies of proteins have been discussed in several excellent reviews.[45–50] Using magnetization transfer techniques such as cross-relaxation-induced polarization transfer (CRIPT) or cross-relaxation-enhanced polarization transfer (CRINEPT), several fold enhancements in intensity can be achieved for systems with molecular masses in excess of 100 kDa.[51,52]

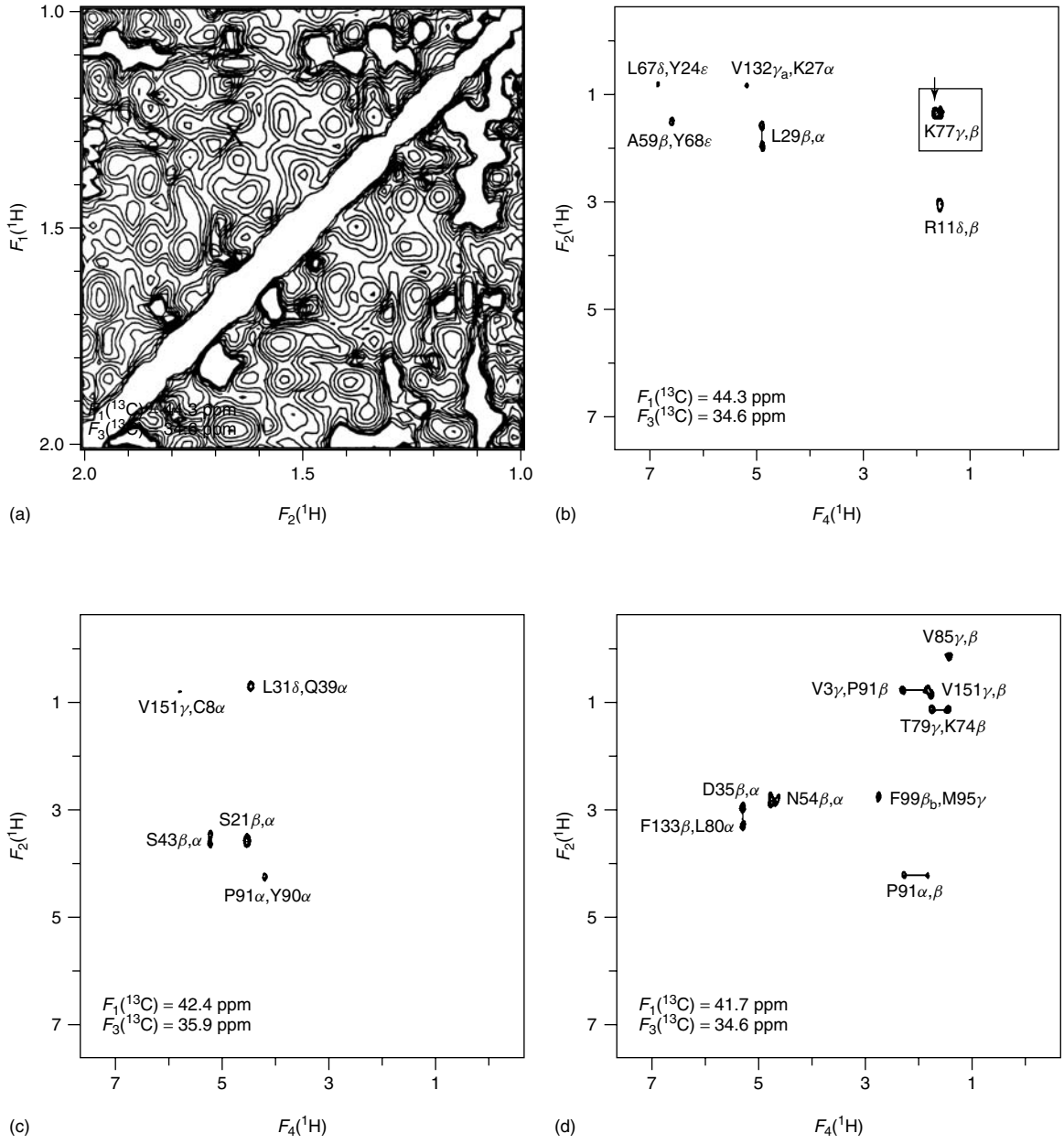
1.0
1.5
2.0
F_1(^{1}H)
2.0
1.5
1.0
F_2(^{1}H)
(a)
L67δ,Y24ε
V132γ_a,K27α
A59β,Y68ε
L29β,α
K77γ,β
R11δ,β
F_1(^{13}C) = 44.3 ppm
F_3(^{13}C) = 34.6 ppm
1
3
5
7
F_2(^{1}H)
7
5
3
1
F_4(^{1}H)
(b)
L31δ,Q39α
V151γ,C8α
S21β,α
S43β,α
P91α,Y90α
F_1(^{13}C) = 42.4 ppm
F_3(^{13}C) = 35.9 ppm
1
3
5
7
F_2(^{1}H)
7
5
3
1
F_4(^{1}H)
(c)
V85γ,β
V3γ,P91β
V151γ,β
T79γ,K74β
D35β,α
N54β,α
F99β_b,M95γ
F133β,L80α
P91α,β
F_1(^{13}C) = 41.7 ppm
F_3(^{13}C) = 34.6 ppm
1
3
5
7
F_2(^{1}H)
7
5
3
1
F_4(^{1}H)
(d)

26.6 CONCLUSION

In this chapter, we have summarized the recent developments in heteronuclear 3D and 4D NMR, which have been designed to extend the NMR methodology to medium-sized proteins in the 15–30 kDa range.[8] The underlying principle of this approach consists of extending the dimensionality of the spectra to obtain significant improvements in spectral resolution while simultaneously exploiting large heteronuclear couplings to circumvent problems associated with larger linewidths. A key feature of all these experiments is that they do not result in any increase in the number of observed cross peaks relative to their 2D counterparts. Hence, the improvement in resolution is achieved without raising the spectral complexity, rendering data interpretation straightforward. Thus, for example, in 4D heteronuclear-edited NOE spectra, the NOE interactions between proton pairs are labeled not only by the ^{1}H chemical shifts but also by the corresponding chemical shifts of their directly bonded heteronuclei in four orthogonal axes of the spectrum. In terms of practical applications, the high sensitivity of these experiments is also important, which makes it feasible to obtain high-quality spectra in a relatively short time frame on 1–2 mM protein samples uniformly labeled with ^{15}N and/or ^{13}C.

Just as 2D NMR opened the application of NMR to the structural determination of small proteins of less than about 100 residues, 3D and 4D heteronuclear NMR provided the means of extending the methodology to medium-sized

Figure 26.5. Comparison of 2D and 4D NMR spectra of interleukin-1β recorded at 600 MHz.[26] The region between 1 and 2 ppm of the 2D NOE spectrum is shown in (a). ^{1}H(F_2)–^{1}H(F_4) planes at several ^{13}C(F_1) and ^{13}C(F_3) frequencies of the 4D ^{13}C/^{13}C NOE spectrum are shown in (b)–(d). No individual cross peaks can be observed in the 2D spectrum and the letter X has ^{1}H coordinates of 1.39 and 1.67 ppm. In contrast, only two cross peaks are observed in the boxed region in (b) between 1 and 2 ppm, one of which (indicated by an arrow) has the same ^{1}H coordinates as the letter X. Further analysis of the complete 4D spectrum reveals the presence of seven NOE cross peaks superimposed at the ^{1}H coordinates of the letter X. This can be ascertained by looking at the ^{13}C(F_1)–^{13}C(F_3) plane taken at the ^{1}H coordinates of X. True diagonal peaks corresponding to magnetization that has not been transferred from one proton to another, as well as intense NOE peaks involving protons attached to the same carbon atom (i.e., methylene protons), appear in only a single ^{1}H(F_2)–^{1}H(F_4) plane of each ^{13}C(F_1), ^{1}H(F_2), ^{1}H(F_4) cube at the carbon frequency where the originating and destination carbon atoms coincide (i.e., at $F_1 = F_3$). Thus, these intense resonances no longer obscure NOEs between protons with similar or degenerate chemical shifts. Two examples of such NOEs can be seen in (c), between the Cα,H protons of Pro-91 and Tyr-90, and (d), between one of the CβH protons of Phe-77 and the methyl protons of Met-95. These various planes of the 4D spectrum also illustrate another key aspect of 3D and 4D NMR, namely, the importance of designing the pulse scheme optimally to remove undesired artifacts that may severely interfere with the interpretation of the spectra. Thus, although the 4D ^{13}C/^{13}C-edited NOESY experiment is conceptually analogous to that of a 4D ^{13}C/^{15}N-edited one, the design of a suitable pulse scheme is actually much more complex in the ^{13}C/^{13}C case. This is due to the fact that there are a large number of spurious magnetization transfer pathways that can lead to observable signals in the homonuclear ^{13}C/^{13}C case. For example, in the 4D ^{15}N/^{13}C-edited case, there are no "diagonal peaks" that would correspond to magnetization that has not been transferred from one hydrogen atom to another, as the double heteronuclear filtering (i.e., ^{13}C and ^{15}N) is extremely efficient at completely removing these normally very intense and uninformative resonances. Such a double filter is not available in the ^{13}C/^{13}C case, and so both additional pulses and phase cycling are required to suppress magnetization transfer through these pathways. This task is far from trivial as the number of phase cycling steps in 4D experiments is severely limited by the need to keep the measurement time down to practical levels (i.e., less than 1 week). The most efficient way of obtaining artifact-free spectra is through the incorporation of pulse field gradients to suppress undesired coherence transfer pathways.[41] Indeed, inclusion of six pulse field gradients into the original pulse scheme of Clore *et al*.[26] reduces the phase cycle from eight to two steps.[42] The results of such care in pulse design can be clearly appreciated from the artifact-free planes shown in (b)–(d). However, when a 4D ^{13}C/^{13}C-edited NOESY spectrum is recorded with the same pulse scheme as that used in the 4D ^{15}N/^{13}C experiment (with the obvious replacement of ^{15}N pulses by ^{13}C pulses), a large number of spurious peaks are observed along a pseudodiagonal at δ^1H(F_2) = δ^1H(F_4) in planes where the carbon frequencies of the originating and destination protons do not coincide. As a result, it becomes virtually impossible under these circumstances to distinguish artifacts from NOEs between protons with the same ^{1}H chemical shifts, as was possible with complete confidence in (c) and (d).

proteins in the 150–300 residue range. Indeed, the determination (in 1991) of the first high-resolution structure of a protein in the 15–20 kDa range, namely, the cytokine interleukin-1β (153 residues and 18 kDa)[53] demonstrated beyond doubt that 3D and 4D NMR permit the structural determination of such medium-sized proteins at a level of accuracy and precision that is comparable to the best results attainable for small proteins. With the following 2 years, several other medium-sized protein structures were determined including protein–peptide and protein–DNA complexes.

REFERENCES

1. K. Wüthrich, *'NMR of Proteins'*, Wiley: New York, 1986,
2. G. M. Clore and A. M. Gronenborn, *Protein Eng.*, 1987, **1**, 275.
3. G. M. Clore and A. M. Gronenborn, *CRC Crit. Rev. Biochem. Mol. Biol.*, 1989, **24**, 479.
4. A. Bax, *Annu. Rev. Biochem.*, 1989, **58**, 223.
5. J. L. Markley, *Methods Enzymol.*, 1989, **176**, 12.
6. K. Wüthrich, *J. Biol. Chem.*, 1990, **265**(22), 059.
7. A. M. Gronenborn and G. M. Clore, *Anal. Chem.*, 1990, **62**, 2.
8. G. M. Clore and A. M. Gronenborn, *Science*, 1991, **252**, 1390.
9. G. M. Clore and A. M. Gronenborn, *Annu. Rev. Biophys. Biophys. Chem.*, 1991, **20**, 29.
10. G. M. Clore, M. A. Robien, and A. M. Gronenborn, *J. Mol. Biol.*, 1993, **231**, 82.
11. G. M. Clore and A. M. Gronenborn, *J. Mol. Biol.*, 1991, **221**, 47.
12. B. Shaanan, A. M. Gronenborn, G. H. Cohen, G. L. Gilliland, B. Veerapandian, D. R. Davies, and G. M. Clore, *Science*, 1992, **257**, 961.
13. H. J. Dyson, G. P. Gippert, D. A. Case, A. Holmgren, and P. E. Wright, *Biochemistry*, 1990, **29**, 4129.
14. J. D. Forman-Kay, G. M. Clore, P. T. Wingfield, and A. M. Gronenborn, *Biochemistry*, 1991, **30**, 2685.
15. H. Oschkinat, C. Griesinger, P. J. Kraulis, O. W. Sørensen, R. R. Ernst, A. M. Gronenborn, and G. M. Clore, *Nature (London)*, 1988, **332**, 374.
16. G. M. Clore and A. M. Gronenborn, *Prog. Nucl. Magn. Reson. Spectrosc.*, 1991, **23**, 43.
17. S. W. Fesik and E. R. P. Zuiderweg, *J. Magn. Reson.*, 1988, **78**, 588.
18. D. Marion, L. E. Kay, S. W. Sparks, D. A. Torchia, and A. Bax, *J. Am. Chem. Soc.*, 1989, **111**, 1515.
19. D. Marion, P. C. Driscoll, L. E. Kay, P. T. Wingfield, A. Bax, A. M. Gronenborn, and G. M. Clore, *Biochemistry*, 1989, **29**, 6150.
20. L. E. Kay, D. Marion, and A. Bax, *J. Magn. Reson.*, 1989, **84**, 72.
21. M. Ikura, A. Bax, G. M. Clore, and A. M. Gronenborn, *J. Am. Chem. Soc.*, 1990, **112**, 9020.
22. G. M. Clore, A. Bax, P. T. Wingfield, and A. M. Gronenborn, *Biochemistry*, 1990, **29**, 5671.
23. M. Ikura, L. E. Kay, R. Tschudin, and A. Bax, *J. Magn. Reson.*, 1990, **86**, 204.
24. E. R. P. Zuiderweg, L. P. McIntosh, F. W. Dahlquist, and S. W. Fesik, *J. Magn. Reson.*, 1990, **86**, 210.
25. L. E. Kay, G. M. Clore, A. Bax, and A. M. Gronenborn, *Science*, 1990, **249**, 411.
26. G. M. Clore, L. E. Kay, A. Bax, and A. M. Gronenborn, *Biochemistry*, 1991, **30**, 12.
27. E. R. P. Zuiderweg, A. M. Petros, S. W. Fesik, and E. T. Olejniczak, *J. Am. Chem. Soc.*, 1991, **113**, 370.
28. G. M. Clore, A. Bax, P. C. Driscoll, P. T. Wingfield, and A. M. Gronenborn, *Biochemistry*, 1990, **29**, 8172.
29. P. C. Driscoll, G. M. Clore, D. Marion, P. T. Wingfield, and A. M. Gronenborn, *Biochemistry*, 1990, **29**, 3542.
30. P. C. Driscoll, A. M. Gronenborn, P. T. Wingfield, and G. M. Clore, *Biochemistry*, 1990, **29**, 4468.
31. A. Bax, G. M. Clore, P. C. Driscoll, A. M. Gronenborn, M. Ikura, and L. E. Kay, *J. Magn. Reson.*, 1990, **87**, 620.
32. S. W. Fesik, H. L. Eaton, E. T. Olejniczak, E. R. P. Zuiderweg, L. P. McIntosh, and F. W. Dahlquist, *J. Am. Chem. Soc.*, 1990, **112**, 886.
33. A. Bax, G. M. Clore, and A. M. Gronenborn, *J. Magn. Reson.*, 1990, **88**, 425.
34. M. Ikura, L. E. Kay, and A. Bax, *Biochemistry*, 1990, **29**, 4659.
35. R. Powers, A. M. Gronenborn, G. M. Clore, and A. Bax, *J. Magn. Reson.*, 1991, **94**, 209.
36. S. Grzesiek and A. Bax, *J. Am. Chem. Soc.*, 1992, **114**, 6291.
37. S. Grzesiek and A. Bax, *J. Biomol. NMR*, 1993, **3**, 185.

38. S. Grzesiek, J. Anglister, and A. Bax, *J. Magn. Reson., Ser. B*, 1993, **101**, 114.
39. S. Grzesiek and A. Bax, *J. Magn. Reson.*, 1992, **99**, 201.
40. G. M. Clore, A. Bax, and A. M. Gronenborn, *J. Biomol. NMR*, 1991, **11**, 13.
41. A. Bax and S. S. Pochapsky, *J. Magn. Reson.*, 1992, **99**, 638.
42. G. W. Vuister, G. M. Clore, A. M. Gronenborn, R. Powers, D. S. Garrett, R. Tschudin, and A. Bax, *J. Magn. Reson., Ser. B*, 1993, **101**, 210.
43. K. Pervushin, R. Riek, G. Wider, and K. Wüthrich, *Proc. Natl. Acad. Sci. U S A*, 1997, **94**, 12366.
44. K. Pervushin, G. Wider, and K. Wüthrich, *J. Biomol. NMR*, 1998, **12**, 345.
45. R. Riek, K. Pervushin, and K. Wüthrich, *Trends Biochem. Sci.*, 2000, **25**, 462.
46. K. Pervushin, *Q. Rev. Biophys.*, 2000, **33**, 161.
47. C. Fernandez and G. Wider, *Curr. Opin. Struct. Biol.*, 2003, **13**, 570.
48. V. Tugarinov, P. M. Hwang, and L. E. Kay, *Annu. Rev. Biochem.*, 2004, **73**, 107.
49. A. G. Tzakos, C. R. Grace, P. J. Lukavsky, and R. Riek, *Annu. Rev. Biophys. Biomol. Struct.*, 2006, **35**, 319.
50. G. Zhu and X. Yao, *Prog. NMR Spectrosc.*, 2008, **30**, 49.
51. R. Riek, G. Wider, K. Pervushin, and K. Wüthrich, *Proc. Natl. Acad. Sci. U S A*, 1999, **96**, 4918.
52. R. Horst, G. Wider, J. Fiaux, E. B. Bertelsen, A. L. Horwich, and K. Wüthrich, *Proc. Natl. Acad. Sci. U S A*, 2006, **103**, 15445.
53. G. M. Clore, P. T. Wingfield, and A. M. Gronenborn, *Biochemistry*, 1991, **30**, 2315.